



Circulation-regulated impacts of aerosol pollution on urban heat island in Beijing

Fan Wang¹, Gregory R. Carmichael², Jing Wang³, Bin Chen⁴, Bo Huang⁵, Yuguo Li⁶, Yuanjian Yang⁷,
and Meng Gao^{1,8}

¹Department of Geography, State Key Laboratory of Environmental and Biological Analysis, Hong Kong
Baptist University, Hong Kong SAR, 999077, China

²Department of Chemical and Biochemical Engineering, The University of Iowa, Iowa City, IA 52242, USA

³Tianjin Key Laboratory for Oceanic Meteorology, and Tianjin Institute of Meteorological Science,
Tianjin 300074, China

⁴Division of Landscape Architecture, Faculty of Architecture, The University of Hong Kong,
Hong Kong SAR, 999077, China

⁵Institute of Space and Earth Information Science and Department of Geography and Resource Management,
The Chinese University of Hong Kong, Hong Kong SAR, 999077, China

⁶Department of Mechanical Engineering, The University of Hong Kong, Pokfulam,
Hong Kong SAR, 999077, China

⁷Collaborative Innovation Centre on Forecast and Evaluation of Meteorological Disasters, Key Laboratory for
Aerosol-Cloud-Precipitation of China Meteorological Administration, School of Atmospheric Physics,
Nanjing University of Information Science and Technology, Nanjing 210044, China

⁸Southern Marine Science and Engineering Guangdong Laboratory (Guangzhou), Guangzhou 511458, China

Correspondence: Meng Gao (mmgao2@hkbu.edu.hk)

Received: 20 March 2022 – Discussion started: 4 April 2022

Revised: 17 August 2022 – Accepted: 14 September 2022 – Published: 18 October 2022

Abstract. Unprecedented urbanization in China has led to serious urban heat island (UHI) issues, exerting intense heat stress on urban residents. Based on the observed temperature and PM_{2.5} concentrations in Beijing over 2016–2020, we find diverse influences of aerosol pollution on urban heat island intensity (UHII) under different circulations. When northerly winds are prevalent in urban Beijing, UHII tends to be much higher in both daytime and nighttime and it is less affected by aerosol concentrations. However, when southerly and westerly winds are dominant in rural Beijing, UHII is significantly reduced by aerosol pollution. Using coupled aerosol-radiation weather simulations, we demonstrate the underlying physical mechanism which is associated with local circulation and resulting spatial distribution of aerosols. Our results also highlight the role of black carbon in aggravating UHI, especially during nighttime. It could thus be targeted for cooperative management of heat islands and aerosol pollution.

1 Introduction

The dramatic global rise of urbanization has led to a rapid growth of urban populations (Elmqvist et al., 2013) and a rapid enlargement of urban sizes (Seto et al., 2012). The massive use of cement and asphalt in urban construction changes local topography and thermal properties of urban surfaces

(Mohajerani et al., 2017; Voogt and Oke, 2010). Coupled with elevated anthropogenic heat and air pollutants from booming human activities, expansion of impervious surface exacerbates urban warming (Grimmond, 2007; Oke, 1982) and degrades diffusion of pollutants (Lewis, 2018; Olivier et al., 2020; Seinfeld, 1989; Zhao et al., 2021), leading to a series of environmental and social issues (Kumar et al., 2017;

Mcdonough et al., 2020). Urbanization has been demonstrated as a critical factor contributing to global warming (Argüeso et al., 2013; Sun et al., 2016; Wilke et al., 2019) and more frequent occurrences of extreme high-temperature events (Sun et al., 2019; Wang and Wang, 2021; Xiao et al., 2022; Zhou et al., 2020). Emissions of trace gases and particles from transportation, industries, and residential activities also threaten health and well-being of urban residents (Crutzen, 2004; Salma et al., 2015; Wilke et al., 2019).

Different surface properties generated by urbanization makes cities warmer than surrounding areas, and urban heat islands (UHI) are thus created by such thermal gradients (Oke, 1973). The UHI is usually calculated as the temperature difference between urban and surrounding rural areas (Deilami et al., 2018). It increases the frequency and intensity of heat waves in urban areas, and thus aggravates heat stress on urban residents (Cao et al., 2016; Li and Bou-Zeid, 2013; Santamouris, 2014). The urban heat island intensity (UHII) is influenced by multiple factors, including ground energy balance, anthropogenic heat release and sky view factors (Oke and Stewart, 2012; Xie et al., 2016a, b). Air pollutants especially aerosols modify surface radiation balance through aerosol radiative effects (ARE), exerting potential impacts on UHII (Cao et al., 2016). The ARE reduce the amount of downward shortwave radiation (SWD) reaching the ground, reduces sensible heat (SH) flux, and lowers the height of the planet boundary layer (PBLH) (Satheesh and Krishnamoorthy, 2005; Yu et al., 2006), which aggravates the severity of haze events in China (aerosol-radiation feedback, ARF, Ding et al., 2016; Gao et al., 2016b; J. Wu et al., 2019; Zhao et al., 2017). The impacts of aerosols on UHI vary with locations, seasons, and day or night (Han et al., 2020). Urban areas are usually the center of pollution with relatively higher aerosol concentrations than rural areas (Seinfeld, 1989). Under this circumstance, aerosols can cut down more SWD and result in stronger reduction of near surface temperature in urban areas, which reduces UHII in daytime (Li et al., 2018; H. Li et al., 2020; Longxun et al., 2003; Sang et al., 2000; Yang et al., 2020). However, absorbing aerosols (e.g., black carbon, BC) absorb and release radiation to increase longwave radiation energy received on urban surfaces, resulting in intensified UHI, especially during nighttime (Cao et al., 2016; Chen et al., 2018; Zheng et al., 2018).

China has been experiencing unprecedented urbanization over the past four decades (Gong et al., 2020; Guan et al., 2018). As the capital city Beijing has achieved a high level of urbanization (Wang et al., 2019; Zhou et al., 2021), leading to serious UHI (Miao et al., 2009; Yang et al., 2013). Although the association between aerosol pollution and UHII in Beijing has been realized, no consensus has been reached (Cao et al., 2016; Li et al., 2020a; Yang et al., 2021, 2020; Yu et al., 2020; Zheng et al., 2018). Yang et al. (2020) and Zheng et al. (2018) found weakened UHI in winter by aerosols in daytime but enhanced during nighttime. Li et al. (2020a) argued that aerosol concentrations in southern rural areas are

usually higher than those in urban or northern rural areas of Beijing, causing a southward shift of UHI. However, Yang et al. (2021) claimed that aerosols increased UHII in winter in Beijing in daytime but weakened it during nighttime. The contradictory results are partly due to the selection of urban and rural monitoring stations, and a detailed explanation with numerical experiments is still lacking. Beijing is located in the North China Plain (NCP), with the Yan Mountains to the northwest and the Bohai Gulf to the southeast. The special topography induces local circulation patterns, such as foehn wind and sea breeze, complicate spatial distribution of near-surface air temperature and aerosol pollution, and thus the influences of aerosol pollution on UHI (Bei et al., 2018; Li et al., 2020b; Q. Wang et al., 2020). The aim of this study is a better understanding of how aerosol pollution affects UHI in Beijing using observations over 2016–2020 and a coupled meteorology-chemistry model. The results would offer valuable information on cooperative management of heat islands and pollution in China.

2 Data and methods

2.1 Observational data

The observed daily average, maximum and minimum temperatures, wind speed and direction from automatic weather stations (AWS) in Beijing over 2016–2020 were obtained from the National Meteorological Information Center (NMIC), China Meteorological Administration (CMA). Preliminary quality control was implemented by the NMIC, and potentially wrong records were checked and corrected (Ren and Xiong, 2007; Ren et al., 2015). We chose two urban stations, Haidian and Guanxiangtai, and the five rural stations Huairou, Shangdianzi, Pinggu, Yanqing and Xiayuling (Fig. S1 and Table S1 in the Supplement) to characterize UHII in Beijing. Hourly PM_{2.5} concentrations over the same period were taken from the China National Environmental Monitoring Center (CNEMC) network.

2.2 Weather research and forecasting model coupled with chemistry configuration

In this study we used the weather research and forecasting model coupled with chemistry (WRF-Chem) version 3.6.1 to explore formation of aerosols and their interactions with radiation and weather (Grell et al., 2005). We configured three domains with grid resolutions of 81, 27 and 9 km. To capture the actual land use types better, we used the moderate resolution imaging spectroradiometer (MODIS) land cover data in 2010 and 2018 (Fig. S1). We used the carbon-bond mechanism version Z (CBMZ, Zaveri and Peters, 1999) and the 8-bin version of the model for simulating aerosol interactions and chemistry (MOSAIC, Zaveri et al., 2008) to simulate gas phase and aerosol chemistry. We added heterogeneous reactions (Gao et al., 2016a) to solve the problem of

underestimation of sulfate. For other options, we followed Wang et al. (2022) to use Lin cloud microphysics (Lin et al., 1983) for cloud microphysics, the Grell 3D ensemble scheme (Grell, 1993) for precipitation, the rapid radiative transfer model (RRTM) (Mlawer et al., 1997) for subgrid longwave radiation and Goddard (Chou et al., 1998) for shortwave radiation. We also used the Noah land surface model (Tewari et al., 2004) for land-atmosphere exchange, Yonsei University planetary boundary layer parameterization (Noh et al., 2006) for boundary layer processes, and the urban canopy model (UCM, Chen et al., 2011) to include the three-dimensional city structure and associated energy balance. For anthropogenic emissions, we used the monthly $0.25^\circ \times 0.25^\circ$ multi-resolution emission inventory for China (MEIC 2010 and MEIC 2018) (Li et al., 2017) in 2010 and 2018. Biogenic emissions were estimated online using the model of emissions of gases and aerosols from nature (MEGAN, Guenther et al., 2006), and we did not include open biomass burning as it was not significant in Beijing during our study period (Gao et al., 2016b). Meteorological initial and boundary conditions were taken from the 6-hourly National Centers of Environmental Prediction (NCEP) final analysis (FNL) dataset.

The difference in heat storage is one important factor that affects the diurnal variation of UHII. In the WRF-Chem model, heat storage is calculated with the land surface model, and we applied the Noah land surface scheme for non-urban grids and the urban canopy model for urban grids. In the Noah land surface scheme, heat storage is calculated using the following equations:

$$G = (1 - F_{\text{veg}}) G_b + F_{\text{veg}} G_v, \quad (1)$$

$$G_b = \frac{2\lambda_{\text{isno}+1}}{\Delta z_{\text{isno}+1}} (T_{g,b} - T_{\text{isno}+1}), \quad (2)$$

$$G_v = \frac{2\lambda_{\text{isno}+1}}{\Delta z_{\text{isno}+1}} (T_{g,v} - T_{\text{isno}+1}), \quad (3)$$

where F_{veg} denotes fractional vegetated area, G_b and G_v are heat storage for bare ground and vegetated ground, respectively, and $\lambda_{\text{isno}+1}$ represents the thermal conductivity of the surface layer (snow or soil), $z_{\text{isno}+1}$ is the layer thickness of the surface layer (snow or soil), $T_{\text{isno}+1}$ represents the temperature of the surface layer of snow (under $\text{isno} + 1 < 0$) or soil (under $\text{isno} = 0$), and $T_{g,b}$ and $T_{g,v}$ stand for ground surface temperature at bare ground fraction and vegetated fraction, respectively. In the urban canopy model, heat storage is calculated using

$$G = G_0 + 2 \int_0^{z_r} \left[\frac{\partial(\rho_b c_b T_b)}{\partial t} \right] dz, \quad (4)$$

where G_0 denotes the surface heat flux into the ground per unit area, z_r is the urban layer, and ρ_b , c_b , and T_b represent the density, specific heat, and temperature of buildings.

2.3 Experimental design

We designed two groups of simulations of a severe haze event in the winter of 2010 (case_2010) and a light pollution event in the spring of 2018 (case_2018). Both cases had four sets of simulations, namely AF, NAF, NBC and Ndust, to explore the impacts of aerosols on UHII, including roles of scattering and absorbing aerosols. The AF cases were performed with actual conditions, while we turned off aerosol-radiation feedbacks in NAF. The NBC was designed as the simulation that ignored the absorption of black carbon (BC) and absorption of dust was turned off in Ndust. In case_2010, the simulation period covered from 11 to 20 January 2010 with the first 5 days as spin-up. The study period included 3 days and nights from 08:00 LST on 16 January to 08:00 LST on 19 January 2010. It covered an entire severe haze pollution event in winter, during which UHI was formed and the wind direction changed over days, providing conditions to analyze the impacts of ARF on UHII under different circulation conditions. In case_2018, the simulation period covered from 19 to 28 April 2018 with the first 5 days as model spin-up time. The study period was from 07:00 LST on 24 April to 07:00 LST on 27 April 2018. It covered a light aerosol pollution in spring and was used to evaluate if the impacts of aerosols on UHII are consistent under different seasons and aerosol pollution conditions. As changes from turning off absorption of dust were negligible, we did not show the results from Ndust in figures.

2.4 Calculation of UHII

We defined UHII_{obs} as observed differences in average 2 m air temperature ($T_{2\text{m}}$) between all urban stations and all rural stations. Following Yang et al. (2020), we also calculated UHII_{max} and UHII_{min} as differences in daily maximum temperature (T_{max}) and daily minimum temperature (T_{min}). As T_{max} often occurs in the afternoon and T_{min} usually happens late at night or in the early morning before sunrise, we used UHII_{max} and UHII_{min} to refer to daytime and nighttime UHII. For simulated UHII, we defined UHII_{sim} as the difference in average $T_{2\text{m}}$ between urban areas and a buffer zone around the urban area that has the same size as the urban area, which is similar to the conditions adopted with satellite products in Zhou et al. (2014). We chose these two different definitions of UHII for observation and simulation to evaluate uncertainty induced by the spatial limitation of monitoring stations.

3 Results and discussion

3.1 Observational evidence of circulation-regulated impacts of aerosol pollution on UHII

Figure 1 presents the probability distributions of UHII under different $\text{PM}_{2.5}$ concentrations. On clean days (daily average $\text{PM}_{2.5}$ concentration below $75 \mu\text{g m}^{-3}$), the distribu-

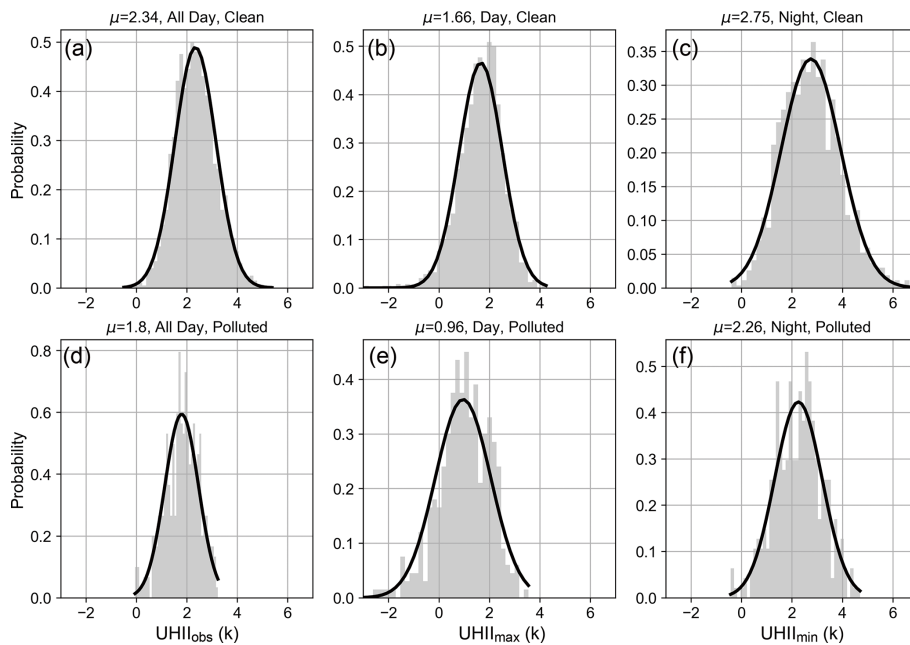


Figure 1. Probability distribution of UHII_{obs} (**a, d**), UHII_{max} (**b, e**) and UHII_{min} (**c, f**) under clean (**a–c**) and polluted (**d–f**) conditions. The bold curve in each subplot is normal distribution curve, and μ denotes the average value.

tion of UHII tends to be more towards larger values with a mean of 2.34 K. It decreases to 1.8 K on pollution days (daily average PM_{2.5} concentration above 75 $\mu\text{g m}^{-3}$) (Fig. 1a, d). UHII exhibits higher values in nighttime than in daytime. In both daytime and nighttime, PM_{2.5} pollution is associated with decreased UHII in Beijing. In this analysis, we calculated the mean PM_{2.5} concentration of all stations (Table S2) in Beijing and used it to determine if Beijing is polluted (daily mean PM_{2.5} concentration $\geq 75 \mu\text{g m}^{-3}$) or clean (daily mean PM_{2.5} concentration $< 75 \mu\text{g m}^{-3}$). We also examined the distribution of daily mean urban and rural PM_{2.5} concentrations under clean and polluted conditions (Table S3), and we found that 17.07 % of clean days at rural stations were classified as polluted ones of urban stations due to the pollution gradient between urban and rural areas. However, these misclassified days were mostly slightly polluted with PM_{2.5} concentrations over 60 $\mu\text{g m}^{-3}$ (Table S3).

We also evaluated how different standards of polluted or clean would affect the results and we included results based on the standard that PM_{2.5} concentrations of all stations in Beijing meet the thresholds of clean or polluted (Fig. S2) and results based on the standard that both average PM_{2.5} concentrations of all urban stations and rural stations meet the criterion (Fig. S3). Compared with Fig. 1 using mean PM_{2.5} concentration of all stations, we found similar distributions and negligible differences in mean values. When PM_{2.5} concentrations of all stations met the criterion, we found the mean values increased by 0.03–0.04 K for clean conditions but decreased by 0.14 K during the daytime and 0.06 K during the nighttime. When we used average PM_{2.5}

concentrations of all urban stations and rural stations to determine clean or polluted conditions, the mean values decreased by 0.01 K for clean conditions and increased by 0.01 and 0.06 K during daytime and nighttime, respectively. We thus believe that using the daily mean PM_{2.5} concentrations averaged over all stations can accurately represent the regional feature of aerosol pollution and would not affect our findings.

It was previously found that aerosol pollution led to decreased UHII_{max} (daytime) but increased UHII_{min} (nighttime) (Yang et al., 2021, 2020). This discrepancy is associated with the differences in regions that were considered as rural in the calculation. We used rural stations located in the west and north of Beijing as rural in the calculation of UHII, and PM_{2.5} concentrations are usually much lower there. As a result the temperature at these rural stations is less affected by aerosol pollution. We designed a simplified flow chart to show how UHII is changed in the daytime and nighttime, assuming that rural areas are not influenced by ARE (Fig. 2). The ARE reduces near surface temperatures in urban areas, leading to a weakened UHII and heat storage throughout the day. Although the strengthened longwave radiation process in nighttime that due to absorption of aerosols in daytime alleviates the reduction of temperature in urban areas, decreased daytime temperature and heat storage release contribute more to near surface temperatures and results in weakened UHII. The increase of UHII due to a strengthened longwave radiation process is smaller than the decrease of UHII caused by reduced temperatures and heat storage release during the daytime (see difference between Fig. 1b, c, e and f).

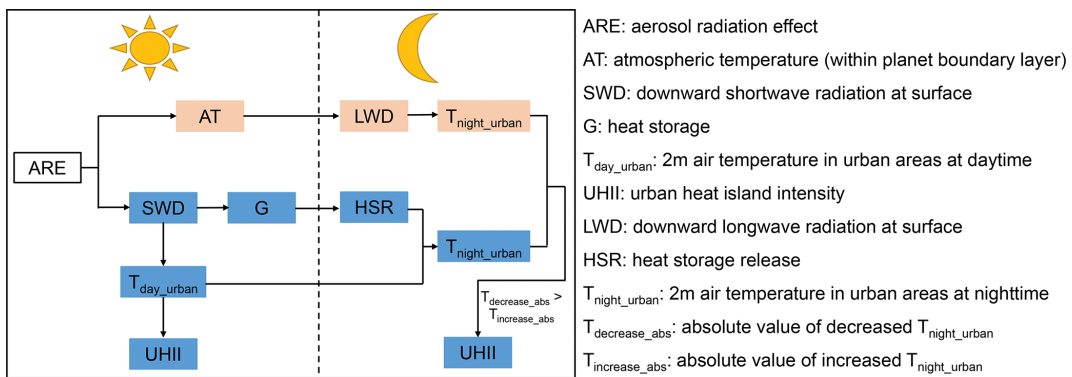


Figure 2. Flow chart showing how UHII is changed in daytime and nighttime, assuming that rural areas are not influenced by ARE. Pink boxes show an increasing trend while blue ones show a decreasing trend.

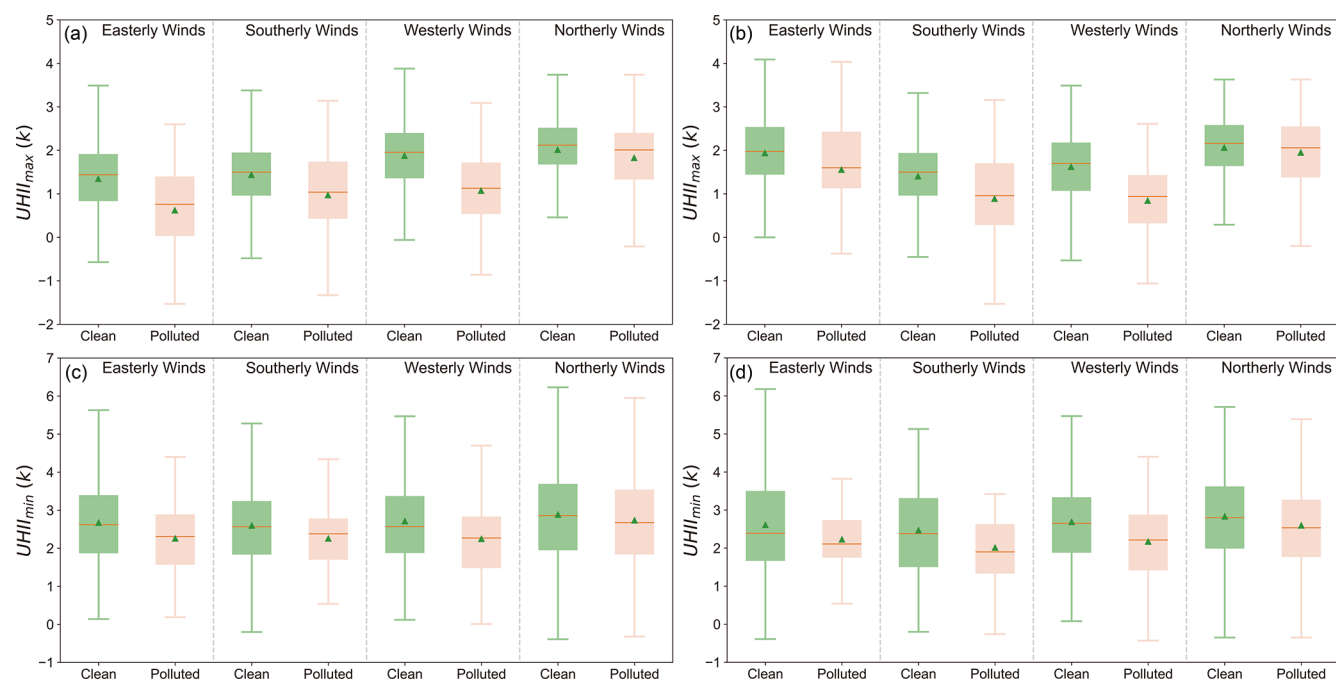


Figure 3. Distribution of UHII under different wind and pollution conditions, (a) and (c) are classified based on the wind direction in urban areas, while (b) and (d) are based on wind direction in rural areas. Green triangles represent average values, red lines are median values, box chart values denote mean values minus standard deviation, 25 % quantile, 75 % quantile, and the mean value plus standard deviation from bottom to top, respectively.

Figure 3 displays the UHII under different wind directions and PM_{2.5} pollution. As the wind direction usually differs in urban areas and rural areas in the west and north of Beijing (Chen et al., 2017), they are discussed separately based on the wind direction in urban sites and rural sites. We observe elevated UHII when northerly winds are prevalent in urban areas on polluted days (Fig. 3a, c). The mean UHII are 2.0 and 1.8 K in daytime and 2.9 and 2.8 K in nighttime on clean and polluted days, respectively. This is associated with reduced aerosol concentrations in urban regions by northerly winds in urban areas (Table 1). From clean to polluted conditions under northerly winds, a lower reduction in UHII by

aerosols is accordingly found (Fig. 3). Larger decreases in UHII in daytime can be found from clean to polluted conditions under easterly, southerly and westerly wind conditions, and these decreases are weakened at nighttime. The weakening may be caused by the longwave radiation process as absorptive aerosols release heat during night to alleviate decreases in surface temperature, especially in urban areas (Cao et al., 2016; Yang et al., 2020). This process has also been confirmed with our simulation that ARE-induced enhanced longwave radiation reduces the weakening of UHII in nighttime (Fig. S4).

Table 1. Average PM_{2.5} concentrations (unit: $\mu\text{g m}^{-3}$) in urban and rural areas under different prevalent wind directions.

Wind directions	Easterly	Southerly	Westerly	Northerly
Urban PM _{2.5}	58.23	53.88	52.24	49.49
Rural PM _{2.5}	50.82	47.34	44.68	43.31

When sorted by wind directions in rural areas, we still find the strongest UHII under northerly wind conditions (Fig. 3b, d). However, UHII is relatively weak and the probability of “cold islands” in daytime increases when westerly or southerly winds are prevalent. The weak UHII under westerly wind conditions is associated with foehn wind that travel northwesterly or westerly through the Yan Mountains, as foehn wind is able to heat rural areas and reduce the urban-rural thermal gradient (Ma et al., 2013). When southerly winds are prevalent, warmer southerly winds from lower latitudes tend to heat southern rural areas faster than urban areas due to blocking of air by buildings and larger heat capacities of urban impervious surfaces and buildings. We also detect larger reductions of UHII by aerosols when westerly or southerly winds are dominant (Fig. 3b, d), suggesting that foehn wind and warm southerly winds are likely to amplify the weakening effect of aerosols on UHII.

3.2 Diurnal variations in the impacts of ARE on UHII

Although we identified consistent weakening of UHII by aerosols during both daytime and nighttime, the influences vary with wind directions, which are regulated by background circulation patterns. To understand the underlying mechanism of the varying influences and to reduce uncertainty induced by selection of monitoring stations, we conducted model simulations of a typical haze event that occurred in winter in Beijing (Gao et al., 2016b) as aerosol concentrations are usually higher in winter in Beijing (Gao et al., 2018). We also designed simulations of a light pollution event in spring to evaluate if the results are robust under different seasons and aerosol pollution conditions. As the aim of this section is to explore the underlying mechanism of interactions between aerosol pollution and urban heat islands, although the period differs from the observations shown above, the selected cases are sufficient to represent the observed varying wind conditions. Model configurations in this study follow Gao et al. (2016b), and extensive model evaluations using multisource observations indicated reliable reproduction of the wintertime haze event (case_2010) by WRF-Chem. We additionally evaluated the performance of WRF-Chem in simulating case_2018 (Fig. S6 and Table S4), and similar results were obtained. Further validation of the ability of the model to simulate site-based UHII is shown in Figs. S7 and S8. The model successfully reproduces the temporal variation of UHII in Beijing, and differences in values

are generally within the trusted range, compared with previous simulations (Li and Bou-Zeid, 2013; Miao et al., 2009). For a better clarification of the influence induced by selection of rural areas, we added Fig. S9 to show the simulated UHII calculated based on site locations and area average. An apparent difference can be found that site-based ΔUHII (difference due to ARE) decreases more than area-based UHII especially in nighttime because of lower PM_{2.5} concentrations in the rural sites than selected rural areas.

Figure 4 shows the temporal variation of UHII of three cases, namely AF, NAF and NBC in case_2010. Given the negligible contribution of absorption of dust to UHII, the results from the Ndust case are not shown. The impacts of ARE on UHII exhibit a bimodal distribution during daytime (Fig. 4a). The first peak and valley appear after sunrise, and the second peak and valley occur before sunset. These variations are associated with the fact that changes in $T_{2\text{m}}$ occur earlier in rural areas. Aerosol pollution cuts down SWD in both urban and rural areas (Fig. S10a, b) after sunrise. Near surface temperature in rural areas usually increases faster than in urban areas (Oke, 1982). As a result, temperatures in rural areas exhibit earlier declines in response to ARE, as indicated by ARE-induced changes in $T_{2\text{m}}$ in Fig. 4b, d, f, g. The second peak is caused by a similar reason that ARE results in the earlier decrease in $T_{2\text{m}}$ in rural areas (Fig. 4b, f), but the release of heat storage also contributes to the second peak. Heat storage of rural areas is usually lower than that of urban areas, yet heat is released more slowly in rural areas, as suggested in Fig. S10 that heat storage is smaller in daytime but reaches zero later than in urban areas (Fig. S10c, d). Heat storage release contributes to upward sensible heat flux at the ground, which further increases $T_{2\text{m}}$ after midday and slows down the decreases after the peak in the afternoon (Oke et al., 1992). As a result, a faster decline of $T_{2\text{m}}$ in rural areas is found than in urban areas (Fig. 4b, f). The ARE reduces heat storage in both rural and urban areas, and the smaller heat storage and slower release of heat in rural areas make $T_{2\text{m}}$ decrease earlier, leading to the second peak and valley. Figure 5 shows related results for case_2018 and we find that ARE generally reduces UHII except on 26 April. The bimodal distribution during daytime still exists but is inconspicuous. This is because the lower ambient PM_{2.5} concentrations in the spring of 2018 reduce the gradient between urban and rural areas, and weaken the impact of ARE on shortwave radiation and near-ground air temperature.

3.3 Diverse influences of ARE on UHII and the role of local circulation

We label days and nights of the study period as D1, N1, D2, N2, D3, N3 in case_2010 and D4, N4, D5, N5, D6, N6 in case_2018 in order, and find diverse influences under different wind patterns. On D1 and N1, we observe that ARE weakens UHII by 0–0.4 K if the absorption of BC is not considered, due to larger amount of scattering aerosols in urban

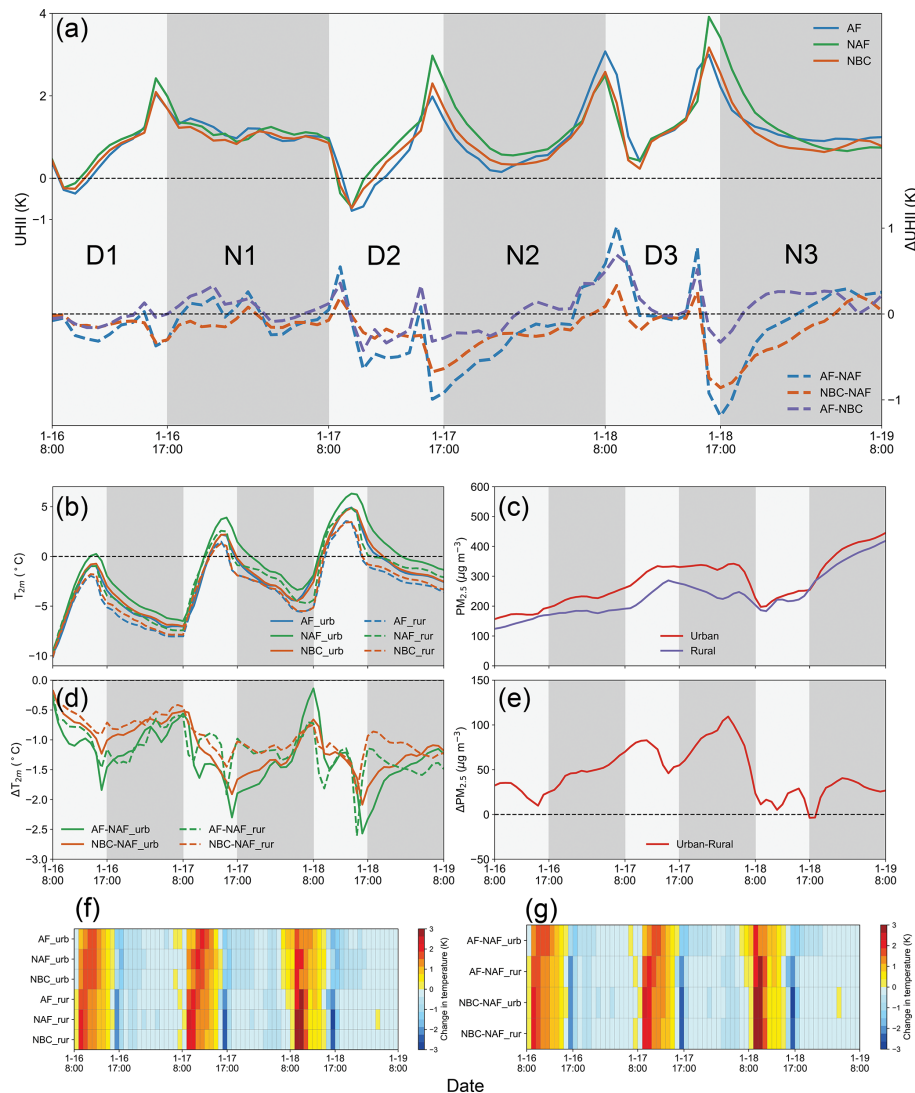


Figure 4. Variations of $UHII_{sim}$ of all cases and differences between them (a) in case_2010. Variations of T_{2m} (b) and ΔT_{2m} (d) in urban and rural areas. Variations of $PM_{2.5}$ (c) and $\Delta PM_{2.5}$ (e) in urban and rural areas of AF case. Hourly changes in T_{2m} (f) and ΔT_{2m} (g) in urban and rural areas, where AF-NAF represents the influence of ARE on UHII, NBC-NAF represents the influence of ARE on UHII by all aerosols but BC and AF-NBC represents the influence of BC absorption on UHII.

areas (Cao et al., 2016; Yang et al., 2020). The weakening is larger in the daytime and UHII is enhanced in the nighttime when absorption of BC is considered (Fig. 4a). BC is potent in absorbing radiation, and it causes larger decreases in SWD in daytime. BC also warms the atmosphere which increases downward longwave radiation (Figs. S11 and S12) in nighttime (Cao et al., 2016; Zheng et al., 2018). On D2, a cold island with an intensity of ~ -0.8 K is formed in Beijing, and ARE enhances the intensity of the cold island. Due to the large reduction of UHII by aerosols in daytime (Fig. 4a), we still find negative effects of ARE on UHII on N2. Yet the negative effects weaken and become positive before sunrise. Different from the previous 2 days, ARE enhances UHII with a maximum value of 1 K on D3. This is associated with

reduced differences in $PM_{2.5}$ concentrations between urban and rural areas on D3 (Figs. 4c and S13c). The conditions on N3 are similar with those on N2. The impacts of aerosols on UHII in nighttime are mainly generated by modified downward longwave radiation (Yang et al., 2021; Zheng et al., 2018), which influences the UHII maintained after sunset. BC is the main light-absorbing aerosol (Gao et al., 2021; Ramanathan and Carmichael, 2008), and higher concentrations of BC (Fig. S11) lead to enhanced UHII in nighttime (Fig. S12). This explains the larger intensified UHII (~ 2 K) on N2. On D4 and D5, due to a much lower $PM_{2.5}$ concentration, ARE reduces UHII by less than 0.2 K (Fig. 5). The lower concentration also diminishes absorption of shortwave radiation during the daytime, which further reduces down-

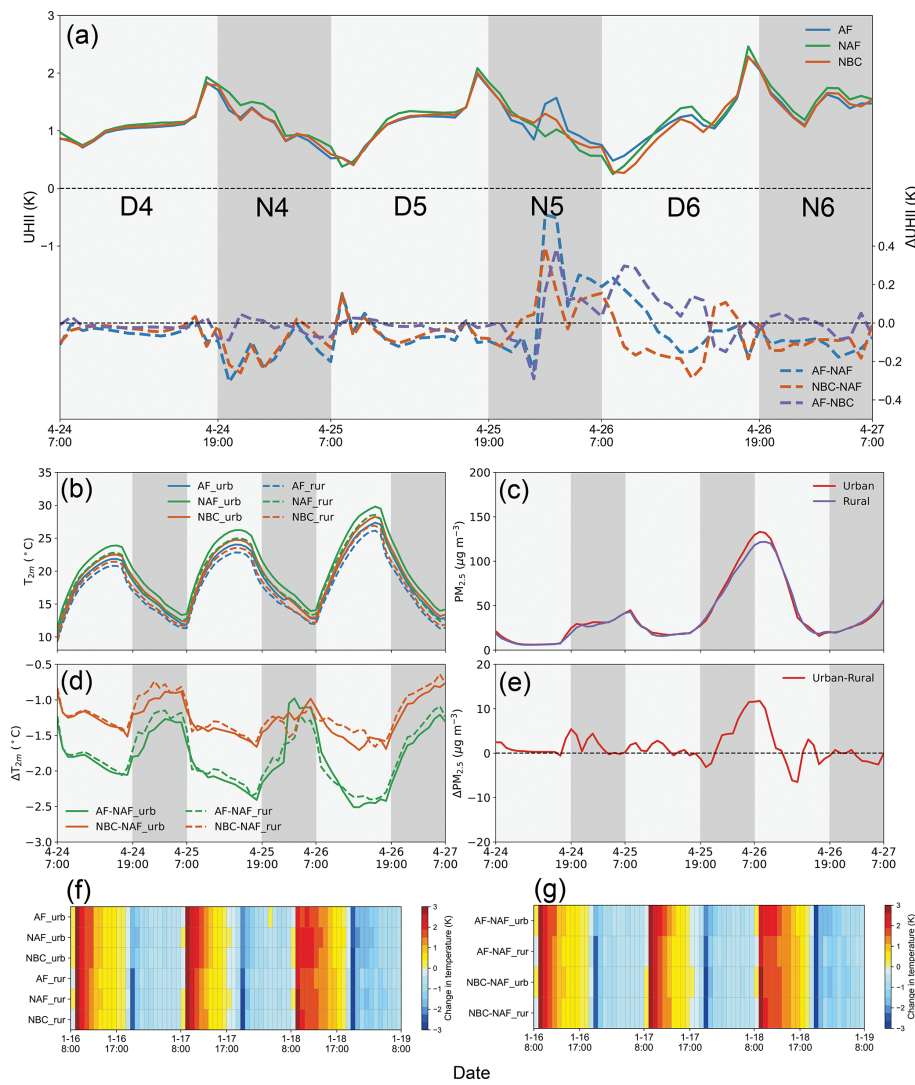


Figure 5. Same as Fig. 4 but for Case_2018.

ward longwave radiation and causes weakened UHII on N4 and N5. On N5, we find a sudden ARE-induced increase in UHII (Fig. 5), and it is associated with the elevated PM_{2.5} concentration on N5 (Fig. 5c).

The abovementioned diverse influences on different days of the study period are mainly controlled by local circulation. Figure 6 presents spatial distributions of daytime 2 m air temperatures and 10 m wind fields over the study period. On D1 (Fig. 6a, d, g), southerly winds dominate the NCP, bringing warmer air to Beijing. However, due to relatively higher PM_{2.5} concentrations in the south of Beijing (Fig. S13), ARE decreases T_{2m} as well as wind speeds. As a result, the warmer air transported from the southern regions to the south of Beijing is weakened, and only southern rural areas can be significantly heated, reducing the UHII of Beijing. This explains why UHII tends to be relatively weaker and there are larger reductions of UHII by aerosols

when southerly winds are prevalent in NCP (Fig. 3). On D2 (Fig. 6b, e, h), strong northwesterly winds (foehn wind) influence Beijing, and the entire western suburbs of Beijing heat up rapidly, forming a cold island. Meanwhile, mountains block strong northwesterly winds, and wind speeds on NCP are relatively weak, favoring accumulation of aerosols in urban areas (Fig. S13). Accordingly, ARE significantly reduces T_{2m} in urban areas and further inhibits the UHII in the west of the city, consistent with the results shown in Fig. 3b that the largest reduction in UHII was caused by aerosol pollution. On D3 (Fig. 6c, f, i), we detect a southeasterly sea breeze coming from the Bohai Gulf. Under the influence of the Yan Mountains, wind directions change to northeasterly when they reach Beijing. Consequently, more aerosols accumulate in the southern rural areas of Beijing (Fig. S13) and ARE contributes to larger decreases in T_{2m} in rural areas than that in urban areas. We thus observe an enhanced UHII

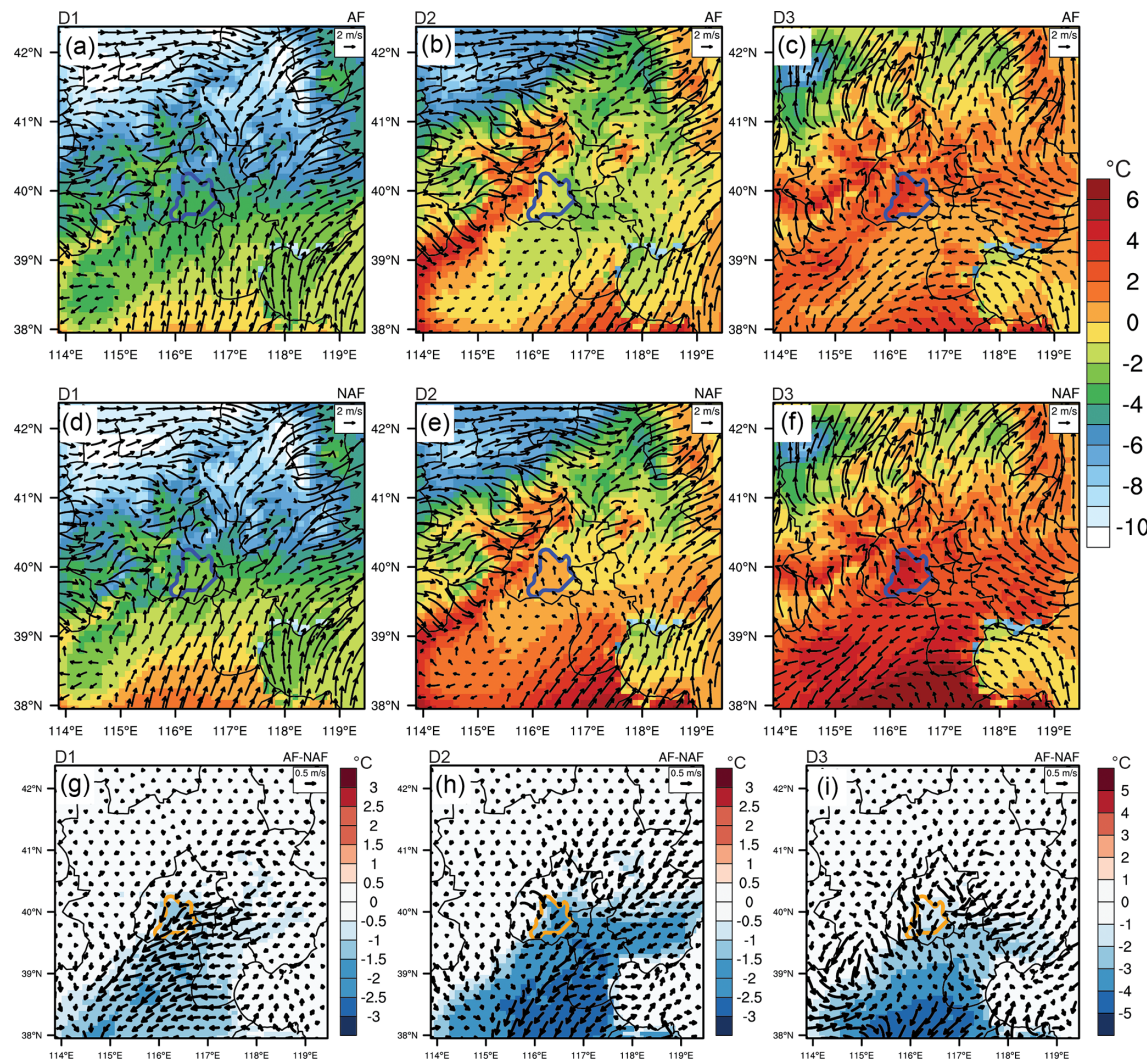


Figure 6. Simulated 2 m air temperatures and 10 sm wind fields in AF (first row), NAF (second row) and differences between AF and NAF (third row) on D1 (first column), D2 (second column), and D3 (third column). The areas within the blue (**a–f**) and orange (**g–i**) line are urban areas of Beijing.

caused by ARE on that day (Fig. 4a). This situation is consistent with observations that the strongest UHII and alleviated reduction of UHII by aerosol pollution occur when urban areas are under northerly winds (Fig. 3a, c). When a slight pollution event happens, similar responses (except results on N5) but smaller values are found (Fig. S14). The identified sudden ARE-induced increase in UHII on N5 (see Fig. 5) is caused by southerly winds. Southerly wind transports warm air masses with high PM_{2.5} concentrations from lower latitude to the north, and this process enhances the downward longwave radiation to heat the surface of urban and southern rural regions, resulting in enhanced UHII (Fig. S15). This also explains why UHII tends to decrease less when southerly winds are prevalent in nighttime (Fig. 3c).

4 Summary

The observed temperatures and PM_{2.5} concentrations in Beijing over 2016–2020 suggest that aerosol pollution is associated with decreased UHII in Beijing in both daytime and nighttime, yet the influences of aerosol pollution on UHII are diverse under different circulation patterns. When northerly winds are prevalent in urban Beijing, UHII tends to be much higher in both daytime and nighttime and it is less affected by aerosol concentrations. The mean values are 2.0 (1.8) and 2.9 (2.8) K in clean (polluted) conditions in daytime and nighttime, respectively. However, when southerly and westerly winds are dominant in rural Beijing, UHII is significantly reduced by aerosol pollution by over 0.5 K. Using coupled aerosol-radiation-weather simulations, we demonstrate the

underlying physical mechanism, which is associated with local circulation and resulting spatial distribution of aerosols.

Previous studies documented opposite effects of aerosol pollution on UHII in Beijing (Cao et al., 2016; Yang et al., 2021, 2020; Yu et al., 2020; Zheng et al., 2018), and other cities (Li et al., 2018; H. Li et al., 2020; Wu et al., 2017; H. Wu et al., 2019). Our study highlights that the influences of aerosol pollution on UHII vary with local circulation, which is particularly important for Beijing due to the complex topography. Besides, heat can be modulated by local circulation to influence the impacts of aerosol pollution on UHII. Therefore, investigating the dominant synoptic patterns in certain areas may contribute to a better understanding of the aerosol-UHII interactions and provide guidance for mitigation strategies (Yang et al., 2020; Yu et al., 2020). Aerosol pollution in China has been significantly alleviated since the implementation of strict clean air policies after 2013 (Gao et al., 2020; Y. Wang et al., 2020). Yet there is still no evidence showing that it has co-benefits of reducing UHI (Li et al., 2007; Cao et al., 2016). It was found that decreasing aerosols led to intensification of urban warming and UHI, which further contributed to aggravation of ozone pollution (Y. Wang et al., 2020; Yu et al., 2020). Thus, controlling aerosol pollution might even pose greater challenges for urban climate and environment management. In this study, our model experiments emphasize the role of BC in aggravating UHI, especially during nighttime (Fig. 4). It could thus be targeted for cooperative management of heat islands and pollution. Some climate and environment friendly measures including urban greening (Chen et al., 2019; Knight et al., 2016) could be adopted to further alleviate both urban heat and air pollution, considering the evapotranspiration effects and extra green space for deposition.

Data availability. The data used in this study can be accessed through contacting the corresponding author.

Supplement. The supplement related to this article is available online at: <https://doi.org/10.5194/acp-22-13341-2022-supplement>.

Author contributions. MG designed the study, and FW performed model simulations and analyzed the data with help from GRC, JW, BC, BH, YL, YY; FW and MG wrote the paper with inputs from all other authors.

Competing interests. The contact author has declared that none of the authors has any competing interests.

Disclaimer. Publisher's note: Copernicus Publications remains neutral with regard to jurisdictional claims in published maps and institutional affiliations.

Financial support. This study was supported by grants from Research Grants Council of the Hong Kong Special Administrative Region, China (project nos. HKBU22201820 and HKBU12202021), National Natural Science Foundation of China (grant no. 42005084) and Natural Science Foundation of Guangdong Province (grant no. 2019A1515011633).

Review statement. This paper was edited by Amos Tai and reviewed by two anonymous referees.

References

- Argüeso, D., Evans, J. P., Fita, L., and Bormann, K. J.: Temperature response to future urbanization and climate change, *Clim. Dynam.*, 42, 2183–2199, <https://doi.org/10.1007/s00382-013-1789-6>, 2013.
- Bei, N., Zhao, L., Wu, J., Li, X., Feng, T., and Li, G.: Impacts of sea-land and mountain-valley circulations on the air pollution in Beijing-Tianjin-Hebei (BTH): A case study, *Environ. Pollut.*, 234, 429–438, <https://doi.org/10.1016/j.envpol.2017.11.066>, 2018.
- Cao, C., Lee, X., Liu, S., Schultz, N., Xiao, W., Zhang, M., and Zhao, L.: Urban heat islands in China enhanced by haze pollution, *Nat. Commun.*, 7, 12509, <https://doi.org/10.1038/ncomms12509>, 2016.
- Chen, F., Kusaka, H., Bornstein, R., Ching, J., Grimmond, C. S. B., Grossman-Clarke, S., Loridan, T., Manning, K. W., Martilli, A., Miao, S., Sailor, D., Salamanca, F. P., Taha, H., Tewari, M., Wang, X., Wyszogrodzki, A. A., and Zhang, C.: The integrated WRF/urban modelling system: development, evaluation, and applications to urban environmental problems, *Int. J. Clim.*, 31, 273–288, <https://doi.org/10.1002/joc.2158>, 2011.
- Chen, Y., An, J. L., Wang, X. Q., Sun, Y. L., Wang, Z. F., and Duan, J.: Observation of wind shear during evening transition and an estimation of submicron aerosol concentrations in Beijing using a Doppler wind lidar, *J. Meteor. Res.*, 31, 350–362, <https://doi.org/10.1007/s13351-017-6036-3>, 2017.
- Chen, L., Zhang, M., Zhu, J., Wang, Y., and Skorokhod, A.: Modeling Impacts of Urbanization and Urban Heat Island Mitigation on Boundary Layer Meteorology and Air Quality in Beijing Under Different Weather Conditions, *J. Geophys. Res.-Atmos.*, 123, 4323–4344, <https://doi.org/10.1002/2017jd027501>, 2018.
- Chen, M., Dai, F., Yang, B., and Zhu, S.: Effects of urban green space morphological pattern on variation of PM_{2.5} concentration in the neighborhoods of five Chinese megacities, *Build. Environ.*, 158, 1–15, <https://doi.org/10.1016/j.buildenv.2019.04.058>, 2019.
- Chou, M.-D., Suarez, M. J., Ho, C.-H., Yan, M. M. H., and Lee, K.-T.: Parameterizations for Cloud Overlapping and Shortwave Single-Scattering Properties for Use in General Circulation and Cloud Ensemble Models, *J. Climate*, 11, 202–214, [https://doi.org/10.1175/1520-0442\(1998\)011<0202:Pfcoas>2.0.Co;2](https://doi.org/10.1175/1520-0442(1998)011<0202:Pfcoas>2.0.Co;2), 1998.
- Crutzen, P.: New Directions: The growing urban heat and pollution “island” effect-impact on chemistry and climate, *Atmos. Environ.*, 38, 3539–3540, <https://doi.org/10.1016/j.atmosenv.2004.03.032>, 2004.

- Deilami, K., Kamruzzaman, M., and Liu, Y.: Urban heat island effect: A systematic review of spatio-temporal factors, data, methods, and mitigation measures, *Int. J. Appl. Earth Observ. Geoinfo.*, 67, 30–42, <https://doi.org/10.1016/j.jag.2017.12.009>, 2018.
- Ding, A. J., Huang, X., Nie, W., Sun, J. N., Kerminen, V. M., Petäjä, T., Su, H., Cheng, Y. F., Yang, X. Q., Wang, M. H., Chi, X. G., Wang, J. P., Virkkula, A., Guo, W. D., Yuan, J., Wang, S. Y., Zhang, R. J., Wu, Y. F., Song, Y., Zhu, T., Zilitinkevich, S., Kulmala, M., and Fu, C. B.: Enhanced haze pollution by black carbon in megacities in China, *Geophys. Res. Lett.*, 43, 2873–2879, <https://doi.org/10.1002/2016gl067745>, 2016.
- Elmqvist, T., Fragkias, M., Goodness, J., Güneralp, B., Marcotullio, P. J., McDonald, R. I., Parnell, S., Schewenius, M., Sendstad, M., Seto, K. C., and Wilkinson, C.: *Urbanization, Biodiversity and Ecosystem Services: Challenges and Opportunities*, Springer Nature, <https://doi.org/10.1007/978-94-007-7088-1>, 2013.
- Gao, M., Carmichael, G. R., Wang, Y., Ji, D., Liu, Z., and Wang, Z.: Improving simulations of sulfate aerosols during winter haze over Northern China: the impacts of heterogeneous oxidation by NO₂, *Front. Environ. Sci. Eng.*, 10, 16, <https://doi.org/10.1007/s11783-016-0878-2>, 2016a.
- Gao, M., Carmichael, G. R., Wang, Y., Saide, P. E., Yu, M., Xin, J., Liu, Z., and Wang, Z.: Modeling study of the 2010 regional haze event in the North China Plain, *Atmos. Chem. Phys.*, 16, 1673–1691, <https://doi.org/10.5194/acp-16-1673-2016>, 2016b.
- Gao, M., Beig, G., Song, S., Zhang, H., Hu, J., Ying, Q., Liang, F., Liu, Y., Wang, H., Lu, X., Zhu, T., Carmichael, G. R., Nielsen, C. P., and McElroy, M. B.: The impact of power generation emissions on ambient PM_{2.5} pollution and human health in China and India, *Environ. Int.*, 121, 250–259, <https://doi.org/10.1016/j.envint.2018.09.015>, 2018.
- Gao, M., Liu, Z., Zheng, B., Ji, D., Sherman, P., Song, S., Xin, J., Liu, C., Wang, Y., Zhang, Q., Xing, J., Jiang, J., Wang, Z., Carmichael, G. R., and McElroy, M. B.: China's emission control strategies have suppressed unfavorable influences of climate on wintertime PM_{2.5} concentrations in Beijing since 2002, *Atmos. Chem. Phys.*, 20, 1497–1505, <https://doi.org/10.5194/acp-20-1497-2020>, 2020.
- Gao, M., Yang, Y., Liao, H., Zhu, B., Zhang, Y., Liu, Z., Lu, X., Wang, C., Zhou, Q., Wang, Y., Zhang, Q., Carmichael, G. R., and Hu, J.: Reduced light absorption of black carbon (BC) and its influence on BC-boundary-layer interactions during "APEC Blue", *Atmos. Chem. Phys.*, 21, 11405–11421, <https://doi.org/10.5194/acp-21-11405-2021>, 2021.
- Gong, P., Li, X., Wang, J., Bai, Y., Chen, B., Hu, T., Liu, X., Xu, B., Yang, J., Zhang, W., and Zhou, Y.: Annual maps of global artificial impervious area (GAIA) between 1985 and 2018, *Remote Sens. Environ.*, 236, 111510, <https://doi.org/10.1016/j.rse.2019.111510>, 2020.
- Grell, G. A.: Prognostic Evaluation of Assumptions Used by Cumulus Parameterizations, *Month. Weather Rev.*, 121, 764–787, [https://doi.org/10.1175/1520-0493\(1993\)121<0764:Peaub>2.0.Co;2](https://doi.org/10.1175/1520-0493(1993)121<0764:Peaub>2.0.Co;2), 1993.
- Grell, G. A., Peckham, S. E., Schmitz, R., McKeen, S. A., Frost, G., Skamarock, W. C., and Eder, B.: Fully coupled "online" chemistry within the WRF model, *Atmos. Environ.*, 39, 6957–6975, <https://doi.org/10.1016/j.atmosenv.2005.04.027>, 2005.
- Grimmond, S.: Urbanization and global environmental change: local effects of urban warming, *Geograph. J.*, 173, 83–88, https://doi.org/10.1111/j.1475-4959.2007.232_3.x, 2007.
- Guan, X., Wei, H., Lu, S., Dai, Q., and Su, H.: Assessment on the urbanization strategy in China: Achievements, challenges and reflections, *Habitat Int.*, 71, 97–109, <https://doi.org/10.1016/j.habitatint.2017.11.009>, 2018.
- Guenther, A., Karl, T., Harley, P., Wiedinmyer, C., Palmer, P. I., and Geron, C.: Estimates of global terrestrial isoprene emissions using MEGAN (Model of Emissions of Gases and Aerosols from Nature), *Atmos. Chem. Phys.*, 6, 3181–3210, <https://doi.org/10.5194/acp-6-3181-2006>, 2006.
- Han, B.-S., Baik, J.-J., Kwak, K.-H., and Park, S.-B.: Effects of cool roofs on turbulent coherent structures and ozone air quality in Seoul, *Atmos. Environ.*, 229, 117476, <https://doi.org/10.1016/j.atmosenv.2020.117476>, 2020.
- Knight, T., Price, S., Bowler, D., and King, S.: How effective is "greening" of urban areas in reducing human exposure to ground-level ozone concentrations, UV exposure and the "urban heat island effect"? A protocol to update a systematic review, *Environ. Evid.*, 5, 3, <https://doi.org/10.1186/s13750-016-0054-y>, 2016.
- Kumar, R., Mishra, V., Buzan, J., Kumar, R., Shindell, D., and Huber, M.: Dominant control of agriculture and irrigation on urban heat island in India, *Sci. Rep.*, 7, 14054, <https://doi.org/10.1038/s41598-017-14213-2>, 2017.
- Lewis, A. C.: The changing face of urban air pollution, *Science*, 359, 744–745, <https://doi.org/10.1126/science.aar4925>, 2018.
- Li, D. and Bou-Zeid, E.: Synergistic Interactions between Urban Heat Islands and Heat Waves: The Impact in Cities Is Larger than the Sum of Its Parts, *J. Appl. Meteorol. Clim.*, 52, 2051–2064, <https://doi.org/10.1175/jamc-d-13-02.1>, 2013.
- Li, H., Meier, F., Lee, X., Chakraborty, T., Liu, J., Schaap, M., and Sodoudi, S.: Interaction between urban heat island and urban pollution island during summer in Berlin, *Sci. Total Environ.*, 636, 818–828, <https://doi.org/10.1016/j.scitotenv.2018.04.254>, 2018.
- Li, H., Sodoudi, S., Liu, J., and Tao, W.: Temporal variation of urban aerosol pollution island and its relationship with urban heat island, *Atmos. Res.*, 241, 104957, <https://doi.org/10.1016/j.atmosres.2020.104957>, 2020.
- Li, J., Zhou, M., Lenschow, D. H., Cheng, Z., and Dou, Y.: Observed Relationships Between the Urban Heat Island, Urban Pollution Island, and Downward Longwave Radiation in the Beijing Area, *Earth Space Sci.*, 7, e2020EA001100, <https://doi.org/10.1029/2020ea001100>, 2020a.
- Li, J., Sun, Z., Lenschow, D. H., Zhou, M., Dou, Y., Cheng, Z., Wang, Y., and Li, Q.: A foehn-induced haze front in Beijing: observations and implications, *Atmos. Chem. Phys.*, 20, 15793–15809, <https://doi.org/10.5194/acp-20-15793-2020>, 2020b.
- Li, M., Liu, H., Geng, G., Hong, C., Liu, F., Song, Y., Tong, D., Zheng, B., Cui, H., Man, H., Zhang, Q., and He, K.: Anthropogenic emission inventories in China: a review, *Nat. Sci. Rev.*, 4, 834–866, <https://doi.org/10.1093/nsr/nwx150>, 2017.
- Lin, Y.-L., Farley, R. D., and Orville, H. D.: Bulk Parameterization of the Snow Field in a Cloud Model, *J. Clim. Appl. Meteorol.*, 22, 1065–1092, [https://doi.org/10.1175/1520-0450\(1983\)022<1065:Bpsotsf>2.0.Co;2](https://doi.org/10.1175/1520-0450(1983)022<1065:Bpsotsf>2.0.Co;2), 1983.
- Longxun, C., Wenqin, Z., Xiuji, Z., and Zijiang, Z.: Characteristics of the heat island effect in Shanghai and its

- possible mechanism, *Adv. Atmos. Sci.*, 20, 991–1001, <https://doi.org/10.1007/bf02915522>, 2003.
- Ma, H., Shao, H., and Song, J.: Modeling the relative roles of the foehn wind and urban expansion in the 2002 Beijing heat wave and possible mitigation by high reflective roofs, *Meteorol. Atmos. Phys.*, 123, 105–114, <https://doi.org/10.1007/s00703-013-0289-x>, 2013.
- McDonough, L. K., Santos, I. R., Andersen, M. S., O'Carroll, D. M., Rutledge, H., Meredith, K., Oudone, P., Bridgeman, J., Goody, D. C., Sorensen, J. P. R., Lapworth, D. J., MacDonald, A. M., Ward, J., and Baker, A.: Changes in global groundwater organic carbon driven by climate change and urbanization, *Nat. Commun.*, 11, 1279, <https://doi.org/10.1038/s41467-020-14946-1>, 2020.
- Miao, S., Chen, F., LeMone, M. A., Tewari, M., Li, Q., and Wang, Y.: An Observational and Modeling Study of Characteristics of Urban Heat Island and Boundary Layer Structures in Beijing, *J. Appl. Meteorol. Clim.*, 48, 484–501, <https://doi.org/10.1175/2008jamc1909.1>, 2009.
- Mlawer, E. J., Taubman, S. J., Brown, P. D., Iacono, M. J., and Clough, S. A.: Radiative transfer for inhomogeneous atmospheres: RRTM, a validated correlated-k model for the longwave, *J. Geophys. Res.-Atmos.*, 102, 16663–16682, <https://doi.org/10.1029/97jd00237>, 1997.
- Mohajerani, A., Bakaric, J., and Jeffrey-Bailey, T.: The urban heat island effect, its causes, and mitigation, with reference to the thermal properties of asphalt concrete, *J. Environ. Manage.*, 197, 522–538, <https://doi.org/10.1016/j.jenvman.2017.03.095>, 2017.
- Noh, Y., Hong, S.-Y., and Dudhia, J.: A New Vertical Diffusion Package with an Explicit Treatment of Entrainment Processes, *Month. Weather Rev.*, 134, 2318–2341, <https://doi.org/10.1175/mwr3199.1>, 2006.
- Oke, T. R.: City size and the urban heat island, *Atmos. Environ.*, 7, 769–779, [https://doi.org/10.1016/0004-6981\(73\)90140-6](https://doi.org/10.1016/0004-6981(73)90140-6), 1973.
- Oke, T. R.: The energetic basis of the urban heat island, *Q. J. Roy. Meteor. Soc.*, 108, 1–24, <https://doi.org/10.1002/qj.49710845502>, 1982.
- Oke, T. R. and Stewart, I. D.: Local Climate Zones for Urban Temperature Studies, *B. Am. Meteorol. Soc.*, 93, 1879–1900, <https://doi.org/10.1175/bams-d-11-00019.1>, 2012.
- Oke, T. R., Zeuner, G., and Jauregui, E.: The surface energy balance in Mexico City, *Atmos. Environ.*, 26, 433–444, 1992.
- Olivier, T., Thebault, E., Elias, M., Fontaine, B., and Fontaine, C.: Urbanization and agricultural intensification destabilize animal communities differently than diversity loss, *Nat. Commun.*, 11, 2686, <https://doi.org/10.1038/s41467-020-16240-6>, 2020.
- Ramanathan, V. and Carmichael, G.: Global and regional climate changes due to black carbon, *Nat. Geosci.*, 1, 221–227, <https://doi.org/10.1038/ngeo156>, 2008.
- Ren, Z. and Xiong, A.-Y.: Operational system development on three-step quality control of observations from AWS (in Chinese), *Meteorol. Month.*, 33, 19–24, 2007.
- Ren, Z., Zhang, Z., Sun, C., Liu, Y., Li, J., Ju, X., Zhao, Y., Li, Z., Zhang, W., and Li, H.: Development of three-step quality control system of real-time observation data from AWS in China (in Chinese), *Meteorol. Mon.*, 41, 1268–1277, 2015.
- Salma, I., Füri, P., Németh, Z., Balásházy, I., Hofmann, W., and Farkas, Á.: Lung burden and deposition distribution of inhaled atmospheric urban ultrafine particles as the first step in their health risk assessment, *Atmos. Environ.*, 104, 39–49, <https://doi.org/10.1016/j.atmosenv.2014.12.060>, 2015.
- Sang, J., Liu, H., Liu, H., and Zhang, Z.: Observational and numerical studies of wintertime urban boundary layer, *J. Wind Eng. Indust. Aerodyn.*, 87, 243–258, [https://doi.org/10.1016/s0167-6105\(00\)00040-4](https://doi.org/10.1016/s0167-6105(00)00040-4), 2000.
- Santamouris, M.: On the energy impact of urban heat island and global warming on buildings, *Energy Build.*, 82, 100–113, <https://doi.org/10.1016/j.enbuild.2014.07.022>, 2014.
- Satheesh, S. and Krishnamoorthy, K.: Radiative effects of natural aerosols: A review, *Atmos. Environ.*, 39, 2089–2110, <https://doi.org/10.1016/j.atmosenv.2004.12.029>, 2005.
- Seinfeld, J. H.: Urban air pollution: state of the science, *Science*, 243, 745–752, <https://doi.org/10.1126/science.243.4892.745>, 1989.
- Seto, K. C., Guneralp, B., and Hutyra, L. R.: Global forecasts of urban expansion to 2030 and direct impacts on biodiversity and carbon pools, *P. Natl. Acad. Sci. USA*, 109, 16083–16088, <https://doi.org/10.1073/pnas.1211658109>, 2012.
- Sun, Y., Zhang, X., Ren, G., Zwiers, F. W., and Hu, T.: Contribution of urbanization to warming in China, *Nat. Clim. Change*, 6, 706–709, <https://doi.org/10.1038/nclimate2956>, 2016.
- Sun, Y., Hu, T., Zhang, X., Li, C., Lu, C., Ren, G., and Jiang, Z.: Contribution of Global warming and Urbanization to Changes in Temperature Extremes in Eastern China, *Geophys. Res. Lett.*, 46, 11426–11434, <https://doi.org/10.1029/2019gl084281>, 2019.
- Tewari, M., Chen, F., Wang, W., Dudhia, J., LeMone, M., Mitchell, K., Ek, M., Gayno, G., and Wegiel, J.: Implementation and verification of the unified NOAH land surface model in the WRF model, 20th Conference on Weather Analysis and Forecasting/16th Conference on Numerical Weather Prediction, Seattle, WA, USA, 11–15, 2004.
- Voogt, J. A. and Oke, T. R.: Effects of urban surface geometry on remotely-sensed surface temperature, *International J. Remote Sens.*, 19, 895–920, <https://doi.org/10.1080/014311698215784>, 2010.
- Wang, F. and Wang, Y.: Potential role of local contributions to record-breaking high-temperature event in Xiamen, China, *Weather Clim. Extr.*, 33, 100338, <https://doi.org/10.1016/j.wace.2021.100338>, 2021.
- Wang, F., Carmichael, G. R., Zhang, X., Xiao, X., and Gao, M.: Pollution severity-regulated effects of roof strategies on China's winter PM_{2.5}, *npj Clim. Atmos. Sci.*, 5, 1–9, 2022.
- Wang, Q., Zhang, C., Ren, C., Hang, J., and Li, Y.: Urban heat island circulations over the Beijing-Tianjin region under calm and fair conditions, *Build. Environ.*, 180, 107063, <https://doi.org/10.1016/j.buildenv.2020.107063>, 2020.
- Wang, Y., Gao, W., Wang, S., Song, T., Gong, Z., Ji, D., Wang, L., Liu, Z., Tang, G., Huo, Y., Tian, S., Li, J., Li, M., Yang, Y., Chu, B., Petaja, T., Kerminen, V. M., He, H., Hao, J., Kulmala, M., Wang, Y., and Zhang, Y.: Contrasting trends of PM_{2.5} and surface-ozone concentrations in China from 2013 to 2017, *Natl. Sci. Rev.*, 7, 1331–1339, <https://doi.org/10.1093/nsr/nwaa032>, 2020.
- Wang, Z., Liang, L., Sun, Z., and Wang, X.: Spatiotemporal differentiation and the factors influencing urbanization and ecological environment synergistic effects within the Beijing-Tianjin-Hebei urban agglomeration, *J. Environ. Manage.*, 243, 227–239, <https://doi.org/10.1016/j.jenvman.2019.04.088>, 2019.

- Wilke, A. B. B., Beier, J. C., and Benelli, G.: Complexity of the relationship between global warming and urbanization – an obscure future for predicting increases in vector-borne infectious diseases, *Curr. Opin. Insect. Sci.*, 35, 1–9, <https://doi.org/10.1016/j.cois.2019.06.002>, 2019.
- Wu, H., Wang, T., Riemer, N., Chen, P., Li, M., and Li, S.: Urban heat island impacted by fine particles in Nanjing, China, *Sci. Rep.*, 7, 11422, <https://doi.org/10.1038/s41598-017-11705-z>, 2017.
- Wu, H., Wang, T., Wang, Q. g., Riemer, N., Cao, Y., Liu, C., Ma, C., and Xie, X.: Relieved Air Pollution Enhanced Urban Heat Island Intensity in the Yangtze River Delta, China, *Aerosol Air Qual. Res.*, 9, 2683–2696, <https://doi.org/10.4209/aaqr.2019.02.0100>, 2019.
- Wu, J., Bei, N., Hu, B., Liu, S., Zhou, M., Wang, Q., Li, X., Liu, L., Feng, T., Liu, Z., Wang, Y., Cao, J., Tie, X., Wang, J., Molina, L. T., and Li, G.: Aerosol–radiation feedback deteriorates the wintertime haze in the North China Plain, *Atmos. Chem. Phys.*, 19, 8703–8719, <https://doi.org/10.5194/acp-19-8703-2019>, 2019.
- Xiao, X., Xu, Y., Zhang, X., Wang, F., Lu, X., Cai, Z., Brasseur, G., and Gao, M.: Amplified upward trend of the joint occurrences of heat and ozone extremes in China over 2013–2020, *B. Am. Meteorol. Soc.*, 103, 1330–1342 <https://doi.org/10.1175/bams-d-21-0222.1>, 2022.
- Xie, M., Liao, J., Wang, T., Zhu, K., Zhuang, B., Han, Y., Li, M., and Li, S.: Modeling of the anthropogenic heat flux and its effect on regional meteorology and air quality over the Yangtze River Delta region, China, *Atmos. Chem. Phys.*, 16, 6071–6089, <https://doi.org/10.5194/acp-16-6071-2016>, 2016a.
- Xie, M., Zhu, K., Wang, T., Feng, W., Gao, D., Li, M., Li, S., Zhuang, B., Han, Y., Chen, P., and Liao, J.: Changes in regional meteorology induced by anthropogenic heat and their impacts on air quality in South China, *Atmos. Chem. Phys.*, 16, 15011–15031, <https://doi.org/10.5194/acp-16-15011-2016>, 2016b.
- Yang, G., Ren, G., Zhang, P., Xue, X., Tysa, S. K., Jia, W., Qin, Y., Zheng, X., and Zhang, S.: PM_{2.5} Influence on Urban Heat Island (UHI) Effect in Beijing and the Possible Mechanisms, *J. Geophys. Res.-Atmos.*, 126, e2021JD035227, <https://doi.org/10.1029/2021jd035227>, 2021.
- Yang, P., Ren, G., and Liu, W.: Spatial and Temporal Characteristics of Beijing Urban Heat Island Intensity, *J. Appl. Meteorol. Clim.*, 52, 1803–1816, <https://doi.org/10.1175/jamc-d-12-0125.1>, 2013.
- Yang, Y., Zheng, Z., Yim, S. Y. L., Roth, M., Ren, G., Gao, Z., Wang, T., Li, Q., Shi, C., Ning, G., and Li, Y.: PM_{2.5} Pollution Modulates Wintertime Urban Heat Island Intensity in the Beijing-Tianjin-Hebei Megalopolis, China, *Geophys. Res. Lett.*, 47, e2019GL084288, <https://doi.org/10.1029/2019gl084288>, 2020.
- Yu, H., Kaufman, Y. J., Chin, M., Feingold, G., Remer, L. A., Anderson, T. L., Balkanski, Y., Bellouin, N., Boucher, O., Christopher, S., DeCola, P., Kahn, R., Koch, D., Loeb, N., Reddy, M. S., Schulz, M., Takemura, T., and Zhou, M.: A review of measurement-based assessments of the aerosol direct radiative effect and forcing, *Atmos. Chem. Phys.*, 6, 613–666, <https://doi.org/10.5194/acp-6-613-2006>, 2006.
- Yu, M., Tang, G., Yang, Y., Li, Q., Wang, Y., Miao, S., Zhang, Y., and Wang, Y.: The interaction between urbanization and aerosols during a typical winter haze event in Beijing, *Atmos. Chem. Phys.*, 20, 9855–9870, <https://doi.org/10.5194/acp-20-9855-2020>, 2020.
- Zaveri, R. A. and Peters, L. K.: A new lumped structure photochemical mechanism for large-scale applications, *J. Geophys. Res.-Atmos.*, 104, 30387–30415, <https://doi.org/10.1029/1999jd900876>, 1999.
- Zaveri, R. A., Easter, R. C., Fast, J. D., and Peters, L. K.: Model for Simulating Aerosol Interactions and Chemistry (MOSAIC), *J. Geophys. Res.*, 113, D13204, <https://doi.org/10.1029/2007jd008782>, 2008.
- Zhao, B., Liou, K. N., Gu, Y., Li, Q., Jiang, J. H., Su, H., He, C., Tseng, H. R., Wang, S., Liu, R., Qi, L., Lee, W. L., and Hao, J.: Enhanced PM_{2.5} pollution in China due to aerosol-cloud interactions, *Sci. Rep.*, 7, 4453, <https://doi.org/10.1038/s41598-017-04096-8>, 2017.
- Zhao, L., Oleson, K., Bou-Zeid, E., Krayenhoff, E. S., Bray, A., Zhu, Q., Zheng, Z., Chen, C., and Oppenheimer, M.: Global multi-model projections of local urban climates, *Nat. Clim. Change*, 11, 152–157, <https://doi.org/10.1038/s41558-020-00958-8>, 2021.
- Zheng, Z., Ren, G., Wang, H., Dou, J., Gao, Z., Duan, C., Li, Y., Ngarukiyimana, J. P., Zhao, C., Cao, C., Jiang, M., and Yang, Y.: Relationship Between Fine-Particle Pollution and the Urban Heat Island in Beijing, China: Observational Evidence, Bound.-Lay. Meteorol., 169, 93–113, <https://doi.org/10.1007/s10546-018-0362-6>, 2018.
- Zhou, C., Chen, D., Wang, K., Dai, A., and Qi, D.: Conditional attribution of the 2018 summer extreme heat over Northeast China: Roles of urbanization, global warming, and warming-induced circulation changes, *B. Am. Meteorol. Soc.*, 99, 107–112, <https://doi.org/10.1175/bams-d-19-0197.1>, 2020.
- Zhou, D., Zhao, S., Liu, S., Zhang, L., and Zhu, C.: Surface urban heat island in China's 32 major cities: Spatial patterns and drivers, *Remote Sens. Environ.*, 152, 51–61, <https://doi.org/10.1016/j.rse.2014.05.017>, 2014.
- Zhou, Y., Chen, M., Tang, Z., and Mei, Z.: Urbanization, land use change, and carbon emissions: Quantitative assessments for city-level carbon emissions in Beijing-Tianjin-Hebei region, *Sustain. Cities Soc.*, 66, 102701, <https://doi.org/10.1016/j.scs.2020.102701>, 2021.